

Structural, electronic, and magnetic properties of the europium chalcogenides: A hybrid-functional DFT study

Martin Schlipf,^{*} Markus Betzinger, Marjana Ležaić, Christoph Friedrich, and Stefan Blügel

Peter Grünberg Institut and Institute for Advanced Simulation, Forschungszentrum Jülich and JARA, 52425 Jülich, Germany

(Received 10 June 2013; revised manuscript received 21 August 2013; published 25 September 2013)

We analyze the structural, electronic, and magnetic properties of the europium chalcogenide series EuX ($X = \text{O, S, Se, and Te}$) using density-functional theory (DFT). To describe the localized $4f$ states of Eu, we utilize the parameter-free PBE0 and HSE hybrid functionals and found a systematic qualitative and quantitative improvement over the conventional local and semilocal functionals. Both hybrid functionals predict the lattice constant and the bulk modulus of all four compounds accurately. The semiconducting behavior, the opening of the band gap, as well as the nature of the band gap across the series is reproduced. By mapping the magnetic interactions to a Heisenberg model up to the next-nearest neighbors, we find the correct trend of the magnetic order of the Eu compounds (in magnetic coupling of the Eu $4f$ moments), from ferromagnetic in EuO to antiferromagnetic in EuTe, with critical temperatures that are in fair agreement with experiment.

DOI: [10.1103/PhysRevB.88.094433](https://doi.org/10.1103/PhysRevB.88.094433)

PACS number(s): 71.15.Ap, 71.15.Mb, 31.15.E-, 77.84.Bw

I. INTRODUCTION

Europium chalcogenides crystallize in the rock-salt structure, where one atomic sublattice is occupied by the Eu atom and the other one by a chalcogen atom (O, S, Se, or Te). All four compounds are semiconducting and exhibit a half-filled Eu $4f$ shell giving rise to a large magnetic moment of $7 \mu_B$.^{1,2} The relative alignment of these moments depends on the chalcogen atom. While EuO and EuS show a ferromagnetic (FM) order with Curie temperature of 69.7 and 16.5 K, respectively,³ the magnetization exhibits a more complex pattern in EuSe,⁴ indicating a subtle competition between a FM and an antiferromagnetic (AFM) order that can be modified by external parameters such as moderate pressure or strain. Replacing Se by Te then finally leads to an AFM magnetic ordering of the localized moments with a Neel temperature of 9.6 K.³ The long-range magnetic order entails a large exchange splitting of the conduction bands, making the EuX series suitable for spin filter applications.^{5,6} Of particular interest is EuO because thin films can be grown lattice matched on Si,⁷⁻⁹ GaN,⁸ yttria-stabilized zirconia,¹⁰ and GaAs.¹¹ However, the Curie temperature of 69 K¹² in EuO impedes a practical application of this material. Fortunately, the Curie temperature of EuO can be manipulated within certain limits with increasing electron concentration that is achieved for example upon doping with Gd,¹³⁻¹⁶ La,¹⁷ and Ce¹⁸ or in Eu rich phases, i.e., at the presence of oxygen defects.^{15,19}

This is in part a consequence of the band structure of the Eu chalcogenides. Most experimental facts are known about the electronic structure of EuO. High-resolution angular-resolved photoemission spectroscopy (ARPES) for the Ce or Gd doped EuO reveals filling of conduction-band states near the X point.²⁰ This indicates that the band gap in EuO is indirect. The direct band gap at the Γ point is much larger than the indirect gap. After a small doping EuO changes from a semiconductor to a semimetal or metal, and the Curie temperature and transport properties change drastically. Studies of stoichiometric EuO have shown that the conduction band of EuO is spin split in its ferromagnetic state and the spin splitting disappears in the paramagnetic state.²¹

A qualitative understanding of the electronic and magnetic properties of the Eu chalcogenides is provided on the basis of the so-called s - f model, which requires a fine adjustment of the band dispersion, the band gap, the intra-atomic, and the interband exchange interaction between localized and extended states.²² The nature as well as the size of the band gap is important if one wants to extract parameters for realistic model calculations²³ from DFT results. This in turn makes the quantitative theoretical description of the europium chalcogenides using density-functional theory (DFT)^{24,25} a challenging task. DFT calculations employing the local-density approximation (LDA) and the generalized-gradient approximation (GGA) predict all four materials to be metallic in evident contradiction to experiment. The LDA and GGA create a spurious self-interaction that is particularly important for localized states and favors their delocalization.²⁶ This affects in europium chalcogenides first and foremost the Eu $4f$ states, which form, according to experiments,³ the highest valence band states, but become metallic in LDA and GGA. This shortcoming can be circumvented by the DFT + U approach²⁷ that allows for an on-site Coulomb repulsion U and a Hubbard exchange J . It has been shown in previous works²⁸⁻³¹ that the DFT + U approach correctly describes the materials of the EuX series as semiconductors. However, the particular choice of the U and J parameter and the atom and angular momentum to which they are applied strongly affects the electronic structure of these compounds. For example, the addition of the Hubbard U correction to the empty Eu $5d$ orbitals proposed by Larson and Lambrecht²⁹ pushes the $5d$ bands up at the X point but not at the Γ point, resulting in a direct band gap in disagreement with experiment. As the oxygen $2p$ states are also localized, Ingle and Elfmov³⁰ employed in addition to the U on the $4f$ states a U on these oxygen states to investigate the impact of epitaxial strain on EuO. These different approaches to choose the U in the DFT + U method limits its predictive power. We note, however, that the constrained RPA approach allows the calculation of the U parameter from first principles.^{32,33} Furthermore, there are efforts to fit the U parameters such that the DFT + U calculation reproduces the band structure obtained with the

GW approximation of many-body perturbation theory. The latter approach has been recently followed by An *et al.* for EuO.³¹ They fitted the U parameter for the Eu $4f$ states such that the band gap and the exchange splitting of the Eu $4f$ states of a QSCGW calculation of EuO are reproduced by the DFT + U calculation. However, with this single U parameter they have not been able to correctly mimic the position of the oxygen $2p$ states and the bandwidth of the Eu $4f$ states.

In this work we investigate the EuX series by using hybrid functionals, in particular, the PBE0³⁴ and HSE³⁵ functional. In contrast to local functionals, hybrid functionals^{36,37} incorporate a fraction of nonlocal Hartree-Fock (HF) exchange. While for both functionals the amount of nonlocal exchange is fixed to 1/4 by theoretical considerations, the HSE functional additionally screens the Coulomb interaction entering in the HF exchange term. The addition of a fraction of HF exchange leads to a partial compensation of the spurious self-interaction error of LDA and GGA. Thus, it can be expected that the hybrid functionals lead to an improved description of the europium chalcogenides. In fact, we demonstrate in this paper that the PBE0 and HSE are superior to the local functionals in the description of the structural, electronic, and magnetic properties of the europium chalcogenides. Hence they provide an excellent alternative to the DFT + U approach overcoming the difficult choice of the optimal U parameter. In particular, we investigate for all four systems the lattice constant, the bulk modulus, the band gap, as well as the bandwidth of the chalcogen p states. Furthermore, by a mapping of our hybrid DFT total energies to a Heisenberg model with nearest and next-nearest neighbor interaction, we determine the strength of the magnetic coupling and the magnetic ordering temperature. We find that both functionals excellently reproduce the experimental low temperature lattice constant for all four materials. PBE0 and HSE consistently predict an indirect band gap, which is formed between the Γ and X point and which gradually increases from EuO to EuTe. Moreover, both functionals capture the qualitative trend from a ferromagnetic order in EuO to an antiferromagnetic one in EuTe, which is accompanied by a lowering of the magnetic ordering temperature.

This paper is organized as follows. In Sec. II we present the computational details of the calculation. We analyze the results of these calculations in Sec. III and draw our conclusions in Sec. IV.

II. COMPUTATIONAL DETAILS

We employ the all-electron full-potential linearized-augmented-plane-wave (FLAPW) method as realized in the FLEUR code,³⁹ in which the hybrid functionals PBE0 and HSE have been recently implemented.^{40,41} The Brillouin zone is sampled by an $8 \times 8 \times 8$ \mathbf{k} -point mesh for all materials and we incorporate one local orbital for the first unoccupied s , p , d , and f states per atom.⁴² All other important numerical parameters for the calculation depend on the particular compound and are listed in Table I.

To determine the bulk modulus and the theoretically optimized lattice constant, we fit the total energies obtained for different lattice constants to a Murnaghan equation of state.⁴³ In addition to the structural properties, we are also interested

TABLE I. Numerical parameters of the FLAPW calculation for the EuX series. In hybrid functional calculations, the mixed product basis (MPB)³⁸ is employed to represent products of wave functions.

	EuO	EuS	EuSe	EuTe
Muffin-tin radii				
Eu atom (a_0)	2.60	3.08	2.85	2.80
X atom (a_0)	2.16	2.41	2.85	2.80
Plane-wave cutoffs				
FLAPW (a_0^{-1})	4.3	4.5	4.7	4.3
MPB (a_0^{-1})	3.1	3.6	3.0	3.4
Angular-momentum cutoffs				
Eu atom, FLAPW	14	12	14	14
X atom, FLAPW	8	10	14	14
Eu atom, MPB	6	6	6	6
X atom, MPB	4	4	4	4
Number of bands	240	270	260	240

in the electronic structure of the EuX series. To compare to experimental measurements usually performed at room temperature, we need an approach to describe the states above the magnetic ordering temperature. Hence, we approximate the eigenvalues in the paramagnetic phase by removing the exchange splitting of the electronic states in the magnetic ground state.⁴⁴ This procedure is justified by the random alignment of the magnetic moments above the ordering temperature, which cannot result in an overall exchange splitting. Finally, we investigate the magnetic ordering temperature from first principles, by evaluating the total energy at the experimental room-temperature lattice constant for three different magnetic configurations: the FM one and two AFM ones, in which the moments alternate along the [001] (AFM-I) and [111] (AFM-II) direction, respectively. The AFM order doubles the size of the unit cell with an accompanying reduction of the Brillouin zone and the \mathbf{k} -point mesh, respectively, used to sample it. The magnetic couplings J_1 and J_2 are determined by mapping the total energies of these three configurations onto a classical Heisenberg model

$$\mathcal{H} = -\frac{1}{2} \sum_i \mathbf{S}_i \left(J_1 \sum_j^{\text{nn}} \mathbf{S}_j + J_2 \sum_j^{\text{nnn}} \mathbf{S}_j \right), \quad (1)$$

with the normalized spin vectors \mathbf{S}_i and \mathbf{S}_j and where the summations run over the nearest neighbors (nn) and the next-nearest neighbors (nnn). The energy difference of the AFM configurations with respect to the FM reference

$$\Delta E_I = E_{\text{AFM,I}} - E_{\text{FM}} = 8J_1, \quad (2)$$

$$\Delta E_{II} = E_{\text{AFM,II}} - E_{\text{FM}} = 6J_1 + 6J_2 \quad (3)$$

converge with smaller numerical cutoffs, if the total energy of FM and AFM state are evaluated within the same unit cell. The ordering temperature is determined in a Monte Carlo (MC) simulation,⁴⁵ in which we simulate a supercell with 8000 spins. We employ 5000 Metropolis steps to relax the random initial configuration to the steady state for a particular temperature. The specific heat of the system exhibits a peak at the critical temperature.

TABLE II. Lattice constants of the europium chalcogenides in Å.

	PBE0	HSE	LDA + U^a	Expt. ^b	Expt. ^c
EuO	5.120	5.120	5.14	5.127	5.141
EuS	5.969	5.970	5.97	5.951	5.968
EuSe	6.194	6.195	6.20	6.176	6.195
EuTe	6.592	6.600	6.60	6.576	6.598

^aReference 29.^bReference 46 at 4.2 K.^cReference 3 at room temperature.

III. RESULTS

A. Structural properties

Europium chalcogenides crystallize in the rock-salt structure. In Table II we compare their lattice constants calculated for the experimental ground-state magnetic structure with the PBE0 and HSE hybrid functional to theoretical²⁹ and experimental^{3,46} results from the literature. The lattice constants obtained from PBE0 and HSE are very similar and in good agreement with those measured in experiment. For EuO the calculated lattice constant agrees best with the low-temperature value of Ref. 46, while it is closer to the room-temperature values of Ref. 3 for the other chalcogenides. However, from a theoretical point of view, we should rather compare with experimental values obtained at low temperatures since our results do not account for thermal expansion effects (and nor does the LDA + U method of Ref. 29) nor for the paramagnetic phase at room temperature. Overall the mean absolute error is smaller than 0.02 Å. Comparing to LDA + U calculations,²⁹ we observe a close agreement between the theoretical results. The largest deviation is found for EuO, where the hybrid-functional values are closer to the experimental low-temperature data than the LDA + U result. In Table III we present the bulk moduli calculated within PBE0 and HSE for the europium chalcogenides. The values tend to match best to the smaller experimental values, but are well within the experimental error bar of 5 GPa. In the PBE0 functional, the materials are slightly stiffer than in the HSE functional.

B. Electronic properties

Next, we focus on the electronic structure of the europium chalcogenides. We evaluate the band structure (Fig. 1) as well as the density of states (DOS) (Fig. 2) by means of Wannier interpolation^{48–50} using the eigenstates and eigenenergies of the self-consistent PBE0 and HSE calculations as input. Although quantitative differences between the different materials

TABLE III. Bulk moduli of the europium chalcogenides in GPa.

	PBE0	HSE	Expt. ^a
EuO	95.8	93.1	91, 92, 107, 110
EuS	52.6	52.3	50, 56, 61
EuSe	47.1	46.7	48, 52, 53
EuTe	38.0	37.8	35.7, 40, 40

^aReference 47.

and the HSE and PBE0 functional exist, several features of the electronic band structure are common in all our calculations: The highest occupied states are formed by the europium 4*f* majority electrons. The valence band maximum is at the Γ point. Well separated below these *f* states, we find the *p* states of the chalcogen atom. The larger the chalcogen atom, i.e., the more nodes exhibited by the *p* electrons, the smaller is the gap between these *p* and the europium 4*f* states. The size of this gap is the same for both hybrid functionals and amounts to 3.0 eV (EuO), 1.8 eV (EuS), 1.3 eV (EuSe), and 0.7 eV (EuTe). Due to the increasing proximity in energy between the *p* and *f* states for the later compounds of the series, the exchange interaction produced by the *f* states becomes increasingly more effective, and the exchange splitting at the Γ point of the *p* states increases across the series from 0.13 eV (0.13 eV) in EuO to 0.68 eV (0.63 eV) in EuTe for the PBE0 (HSE) functional.

Focusing on the 4*f* states (Table IV) we realize that the exchange splitting, i.e., the energy difference between the minority and majority 4*f* state, is basically independent of the compound, despite some significant changes of their lattice constants. For the PBE0 (HSE) functional the values vary between 11.9 eV (11.0 eV) in EuO and 11.7 eV (10.8 eV) in EuTe. Thus, the exchange splitting obtained from HSE is about 1 eV smaller than that of PBE0. The chemical and structural insensitivity of the exchange splitting can be explained by the intra-atomic Coulomb interaction between the 4*f* electrons of the half-filled shell. Due to the spatial localization of the 4*f* shell, this intra-atomic Coulomb interaction depends little on the screening by other electrons and thus on the type of compound. For example, for metallic bulk Eu, which is in the language of the Coulomb interaction a representative of the fully screened case, an exchange splitting of the 4*f* states of 11 eV⁵¹ was found by combining data of XPS and BIS experiments. Gd*X* monpnictides ($X = P, As, Sb, Bi$) exhibit an 4*f* exchange splitting of 14.5 eV.⁵² Considering that the Coulomb interaction of Eu is about 1 eV smaller than for Gd, our exchange splittings are in the right ballpark between 11 and 13.5 eV and significantly smaller than the LDA + U values²⁹ that are between 16.8 eV (EuTe) and 18 eV (EuO) obtained employing $U_f = 7.397$ eV, $J_f = 1.109$ eV, $U_d = 3.4$ eV, and $J_d = 0$ eV for the Eu 4*f* and 5*d* states, respectively.

The lowest conduction bands are formed by Eu 6*s* and 5*d* states. For all compounds the global minimum is found at the X point and a local minimum at the Γ point. The lowest conduction-band states at the X point exhibit europium t_{2g} character, whereas the 6*s* electrons form the minimum at Γ . The conduction band is subject to a large exchange splitting induced by the localized moments of the 4*f* electrons. In Ref. 21 the exchange splitting was deduced from an investigation of the redshift associated with a cooling from the paramagnetic phase to the ferromagnetic phase in optical absorption experiments. The observed redshifts of 0.225 eV in EuO, 0.18 eV in EuS, and 0.335 eV in EuSe should be roughly equal to half of the exchange splitting. More recently, Steenekens *et al.*⁵³ employed spin-resolved x-ray absorption spectroscopy to measure the exchange splitting of EuO directly. Within the bottom 2 eV of the conduction band, the majority and minority states are found to be split by 0.6 eV. In fact, when we compare the majority and minority DOS of EuO

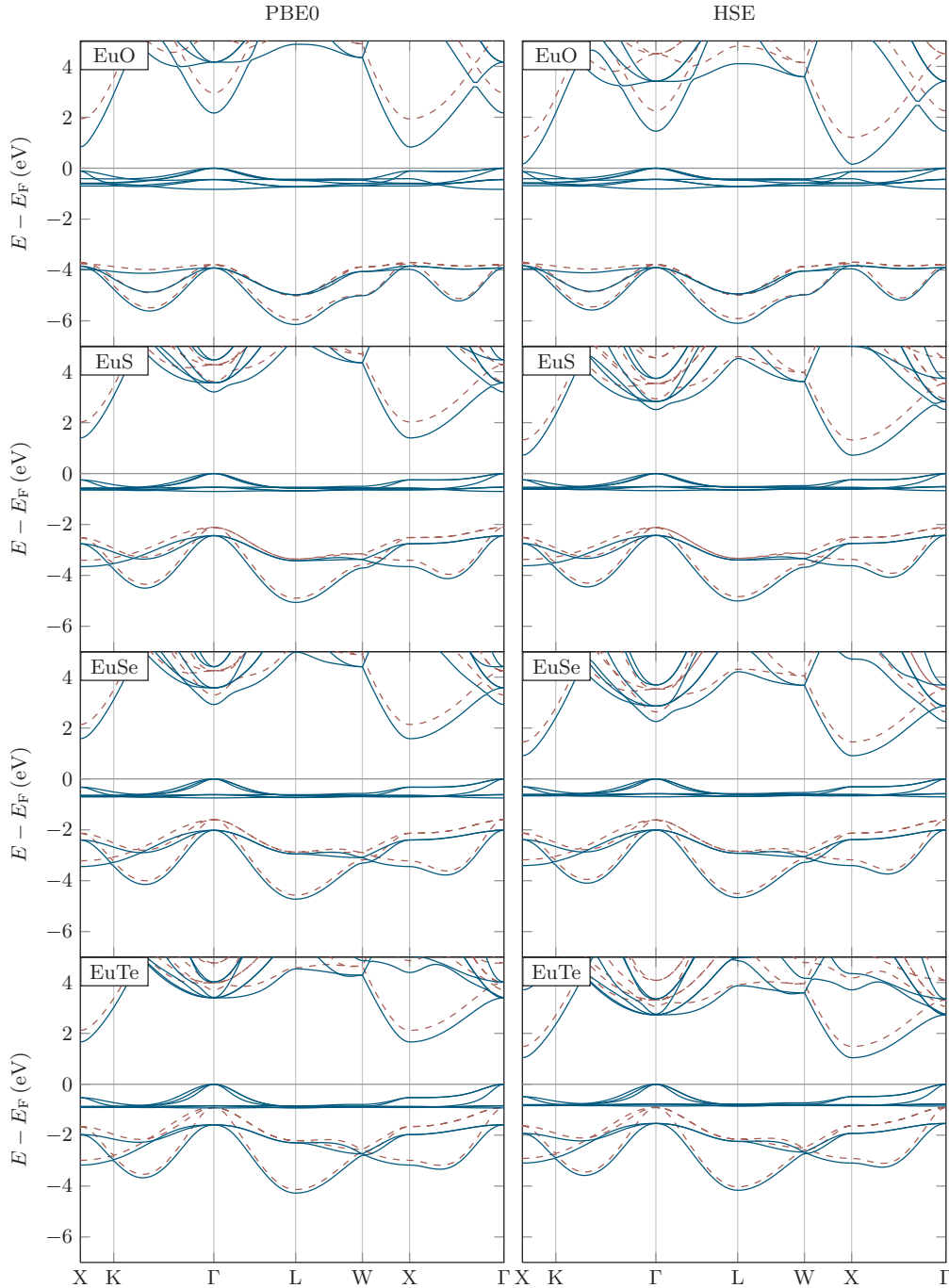


FIG. 1. (Color online) Electronic band structure of the europium chalcogenides. The energies of the bands with respect to the Fermi energy E_F are evaluated with the PBE0 (left column) and HSE (right column) hybrid functional. Majority and minority bands are shown as solid (blue) and dashed (red) lines, respectively.

obtained with the PBE0 (HSE) functional in the experimentally investigated energy range, we find an exchange splitting of 0.56 eV (0.59 eV) in very good agreement with experiment. The values for the other compounds are 0.37 eV (0.38 eV) for EuS, 0.35 eV (0.37 eV) for EuSe, and 0.36 eV (0.35 eV) for EuTe. We note that the exchange splitting at the X point, i.e., at the bottom of the conduction band, is noticeably larger than the average value (see Fig. 1), which we attribute to a pronounced \mathbf{k} dependence of the nonlocal PBE0 (HSE) potential.

In Fig. 2 we compare the nonlocal hybrid functionals to the local PBE-GGA⁵⁴ functional. We recognize that the DOS of the chalcogen p states is almost independent of the applied functional. However, the closing of the gap between these p states and the europium $4f$ states for the larger chalcogen atoms is not captured in PBE. Next, we draw the reader's attention to the position of the Eu $4f$ majority states. In the local PBE functional, the conduction band consisting of Eu $5d$ and $6s$ states overlaps with the $4f$ state, giving rise to a metallic

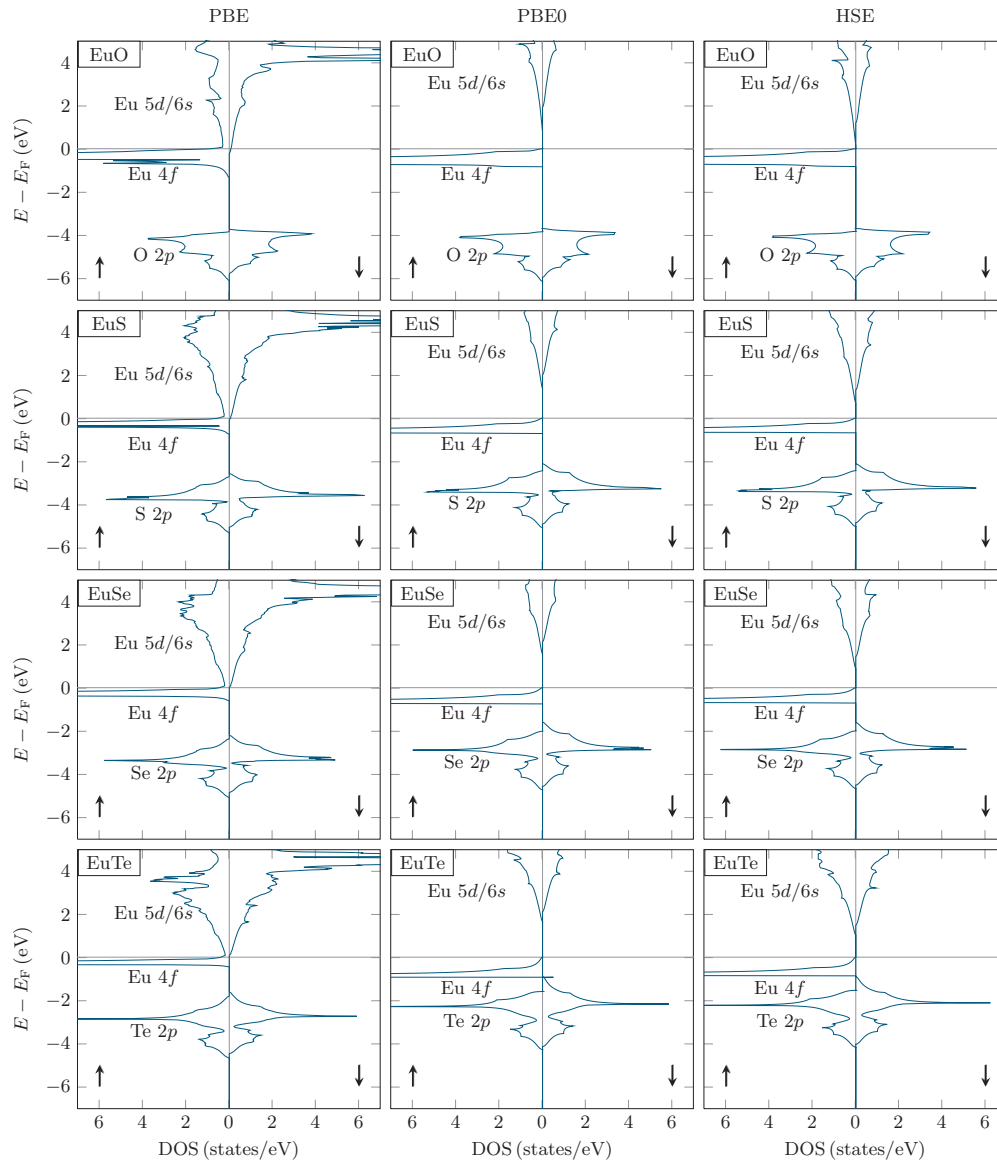


FIG. 2. (Color online) Spin-resolved electronic density of states (DOS) of the europium chalcogenides calculated with the local PBE functional and the hybrid functionals PBE0 and HSE. Please notice the Eu 4*f* minority states as calculated with the hybrid functionals exhibit an exchange splitting of about 11.3 eV and are thus out of the scale.

state. In contrast to this, the hybrid exchange-correlation functionals predict a semiconducting ground state, because the conduction band states are shifted towards higher energies.

In Table IV we summarize band transition energies in the europium chalcogenides. As we already demonstrated in Fig. 2, the local PBE functional is not suitable to describe the ground state of the EuX series. Hence, we compare our hybrid functionals results only to other theoretical²⁹ and experimental^{3,47} results from the literature. To compare the EuX compounds within the series, all transitions were evaluated for a ferromagnetic state, even though EuTe orders AFM experimentally. First, we focus on the differences between the PBE0 and HSE functional. For all materials in the series and independent of the point in the Brillouin zone, we notice that PBE0 predicts roughly 0.7 eV larger values than HSE. This can be attributed to the removal of the

long-range part of the HF exchange in the latter functional. This shift of the conduction band is nearly dispersionless and a similar magnitude is observed in other semiconducting materials as well.⁵⁵ Comparing to experimental observations, we find that the PBE0 functional is better suited to describe the experimental transitions at low temperatures.²¹ Experimentally the direct band gap increases above the magnetic ordering temperature,⁴⁷ and hence it lies almost exactly in between the values calculated with hybrid functionals.

Comparing the transition from the lower lying chalcogen *p* states to the conduction band, we find for EuO a good agreement with x-ray absorption and emission spectroscopy,⁴⁷ where this gap is determined between the highest occupied (here spin-down) and the lowest unoccupied (here spin-up) state. For the materials with heavier chalcogen atoms, although the qualitative trend towards less strongly bound *p* states across

TABLE IV. Band transitions in the europium chalcogenides from highest valence to the lowest conduction band (CB) and from the chalcogen p states to the CB. All values of the transitions in ferromagnetic (FM) phase, which are evaluated for the majority channel, and in the paramagnetic (PM) phase are given in eV. The peak position of the majority and minority f states are given relative to the Fermi energy in eV.

	This work		LDA + U^a		Expt. ^b	This work		LDA + U^a		Expt. ^b
	PBE0	HSE	No U_d	With U_d		PBE0	HSE	No U_d	With U_d	
EuO										
FM Γ - Γ	2.13	1.42	0.68	0.64		3.22	2.52	1.68	1.75	
PM Γ - Γ	2.52	1.81	1.02	0.97		3.42	2.73	1.87	1.94	
FM Γ -X	0.91	0.23	0.15	0.98		1.43	0.74	1.54	2.49	
PM Γ -X	1.45	0.75	0.57	1.31		1.74	1.04	1.90	2.84	
FM X-X	1.02	0.36	0.32	1.17	0.95	1.68	0.99	1.83	2.82	1.51
PM X-X	1.56	0.88	0.75	1.58	1.12	1.99	1.29	2.19	3.17	1.65
p -CB	4.54	3.85		3.3 [†]	3.9, 4.1	3.51	2.84		3.1 [†]	2.3
Bandwidth p	2.26	2.23			3.0	2.30	2.25			2.3
4 f majority	-0.59	-0.58		-0.64		-0.61	-0.58		-0.71	
4 f minority	11.3	10.4		17.4		11.1	10.3		16.7	
EuS										
FM Γ - Γ	2.92	2.25	1.44	1.50		3.40	2.70	1.94	1.96	
PM Γ - Γ	3.11	2.44	1.62	1.88		3.56	2.88	2.09	2.11	
FM Γ -X	1.58	0.91	1.76	2.71		1.67	1.01	2.01	2.92	
PM Γ -X	1.86	1.18	2.09	3.05		1.89	1.23	2.35	3.22	
FM X-X	1.90	1.22	2.13	3.14	1.48, 1.61 ^c	2.19	1.49	2.57	3.58	
PM X-X	2.18	1.49	2.48	3.48	1.78, 1.80	2.42	1.71	2.91	3.88	2.0
p -CB	3.18	2.52		2.5 [†]	2.1	2.57	1.95		2.4 [†]	2.3
Bandwidth p	2.33	2.28			2.2	2.30	2.25			2.3
4 f majority	-0.68	-0.64		-0.83		-0.88	-0.81		-1.14	
4 f minority	11.0	10.2		16.9		10.8	10.0		15.7	
EuSe										
FM Γ - Γ	2.92	2.25	1.44	1.50		3.40	2.70	1.94	1.96	
PM Γ - Γ	3.11	2.44	1.62	1.88		3.56	2.88	2.09	2.11	
FM Γ -X	1.58	0.91	1.76	2.71		1.67	1.01	2.01	2.92	
PM Γ -X	1.86	1.18	2.09	3.05		1.89	1.23	2.35	3.22	
FM X-X	1.90	1.22	2.13	3.14	1.48, 1.61 ^c	2.19	1.49	2.57	3.58	
PM X-X	2.18	1.49	2.48	3.48	1.78, 1.80	2.42	1.71	2.91	3.88	2.0
p -CB	3.18	2.52		2.5 [†]	2.1	2.57	1.95		2.4 [†]	2.3
Bandwidth p	2.33	2.28			2.2	2.30	2.25			2.3
4 f majority	-0.68	-0.64		-0.83		-0.88	-0.81		-1.14	
4 f minority	11.0	10.2		16.9		10.8	10.0		15.7	
EuTe										
FM Γ - Γ	2.92	2.25	1.44	1.50		3.40	2.70	1.94	1.96	
PM Γ - Γ	3.11	2.44	1.62	1.88		3.56	2.88	2.09	2.11	
FM Γ -X	1.58	0.91	1.76	2.71		1.67	1.01	2.01	2.92	
PM Γ -X	1.86	1.18	2.09	3.05		1.89	1.23	2.35	3.22	
FM X-X	1.90	1.22	2.13	3.14	1.48, 1.61 ^c	2.19	1.49	2.57	3.58	
PM X-X	2.18	1.49	2.48	3.48	1.78, 1.80	2.42	1.71	2.91	3.88	2.0
p -CB	3.18	2.52		2.5 [†]	2.1	2.57	1.95		2.4 [†]	2.3
Bandwidth p	2.33	2.28			2.2	2.30	2.25			2.3
4 f majority	-0.68	-0.64		-0.83		-0.88	-0.81		-1.14	
4 f minority	11.0	10.2		16.9		10.8	10.0		15.7	

^aReference 29; [†]extracted from the band structures.

^bReferences 3, 47, and 21.

^cFirst value extrapolated, second value at $T = 2.75$ K.

the series is reproduced, the binding energy of these p states is overestimated in EuS and EuSe by the PBE0 functional and in EuS by the HSE functional. Hybrid functionals give bandwidths of these states that are almost independent of the material, which resembles the experimental observations³ except for EuO, where a larger bandwidth is measured. For the heavier chalcogenides, the experimental bandwidth of roughly 2.3 eV is accurately reproduced.

Next, we focus on the nature and size of the band gap. The LDA + U method²⁹ is not suitable to predict the nature of the band transition. For $U_d = 0$, the band gap changes from an indirect Γ -X transition in EuO and EuS to a direct Γ - Γ one in EuSe and EuTe. With a Hubbard U parameter of 3.4 eV determined from a fit to empirical data for the d states in the electronically similar GdN system, the smallest band transition is a direct one for all materials. However, we notice that the hybrid functionals predict a significantly different picture. The band gap is always associated to the indirect Γ -X transition and the smallest optical band gap is found at the X point. The results of the hybrid functional calculations are in good agreement with recent ARPES measurements²⁰ in Gd-doped EuO. In the LDA + U scheme as well as in our calculations, the direct Γ - Γ transition does not monotonously increase across the series. However, since this transition corresponds to the fundamental band gap in the LDA + U approach, the experimental trend of a monotonous opening of the band gap

is not reproduced, whereas hybrid functionals yield the trend correctly.

Overall, we find that the hybrid functionals yield a very good description of the band structure of the EuX series. The small differences to experimental results in the size of the band gap, the exchange splitting, the distance of the p and the conduction band, and the bandwidth of these p states can be attributed to deviations in the charge-transfer gap of p states and conduction band and the relative position of the 4 f states. To give an estimate on the error bars of our results, we repeated the calculation of EuO with a different amount of HF exchange. A 5% larger amount of HF exchange goes along with a decrease of the gap between p and f states by 0.1 eV, an increase of the band gap by 0.6 eV, and a slight reduction of the exchange splitting by 0.03 eV. The bandwidth of the oxygen p states does not change.

C. Magnetic properties

In this section we focus on the thermodynamical magnetic properties of the europium chalcogenides. Table V lists the exchange coupling constants determined with hybrid functionals, the LDA + U approach,^{28,29} and measured experimental data.⁵⁶ Results of PBE calculations are not shown, because the exchange interaction parameters are totally off. They are way too large and have partly the wrong sign, and for all compounds

TABLE V. Heisenberg exchange coupling constants for nearest (J_1) and next-nearest neighbors (J_2) in meV.

		PBE0	HSE	LDA + U^a	LDA + U^b				Expt. ^c		
J_1	EuO	2.37	2.52	1.95	1.75	1.44	1.64	1.71	2.04	2.06	
	EuS	0.86	0.91	0.62	0.56	0.54	0.58	0.60	0.62	0.64	
	EuSe	0.57	0.50	0.30	0.39	0.30	0.35				
	EuTe	0.32	0.34	-0.01	0.15	0.08	0.12	0.16	0.19	0.27	
J_2	EuO	0.80	0.89	0.60	0.45	-0.30	-0.26	-0.19	0.32	0.71	
	EuS	-0.16	-0.11	-0.68	-0.15	-0.33	-0.32	-0.27	-0.22	-0.16	
	EuSe	-0.35	-0.50	-0.92	-0.29	-0.30	-0.24				
	EuTe	-0.57	-0.56	-1.06	-0.43	-0.58	-0.57	-0.54	-0.41		

^aReference 29.^bExtracted from Figs. 1 and 2 from Ref. 28 for $U_f = 6$ eV.^cReference 56.

the ferromagnetic order is predicted with unrealistically high Curie temperatures. In contrast to this, the results of the hybrid functional calculations provide a rather accurate description of the experimental measurements. The trend in size of the nearest (J_1 , nn) and next-nearest neighbor (J_2 , nnn) exchange interaction as well as the change of sign of the J_2 across the series is accurately described, albeit the coupling constants are larger than the experimentally determined ones. We notice that the different experiments reported in Ref. 56 feature a large uncertainty of the coupling constants.

Comparing the theoretical results, we find that within the limits of the accuracy of our calculations, both hybrid functionals predict the same values for J_1 and J_2 . In contrast to the LDA + U results,²⁹ the nn interaction remains ferromagnetic and is stronger than the nnn interaction for the compounds with a ferromagnetic ground state (EuO and EuS). For EuSe, J_1 and J_2 exhibit a different sign, while their absolute value is about the same, leading to a complex magnetic ordering.⁴ A refined theoretical description for EuSe would require more neighbors to be taken into account.

Kuneš *et al.*²⁸ report exchange constants closer to the experimental values employing a $U = 6$ eV in a LDA + U calculation. However, they point out that these values are subject to a drastic decrease of up to 50%, when increasing the U to 9 eV.

In Table VI we present the ordering temperature of the europium chalcogenides obtained by Monte Carlo (MC) simulations employing the calculated coupling constants. The

TABLE VI. Magnetic ordering temperatures of the EuX series in K, where the arrows indicate a ferromagnetic ($\uparrow\uparrow$) and antiferromagnetic ($\uparrow\downarrow$) alignment. Theoretical values are extracted from a Monte Carlo (MC) simulation.

	PBE0	HSE	LDA + U^a	Expt. ^b
EuO	107 $\uparrow\uparrow$	115 $\uparrow\uparrow$	85 $\uparrow\uparrow$	69.7 $\uparrow\uparrow$
EuS	28 $\uparrow\uparrow$	31 $\uparrow\uparrow$	7 $\uparrow\downarrow$	16.5 $\uparrow\uparrow$
EuSe	12 $\uparrow\uparrow$	4 $\uparrow\uparrow^c$		2.8 $\uparrow\uparrow$
		4 $\uparrow\downarrow^c$	15 $\uparrow\downarrow$	4.6 $\uparrow\downarrow$
EuTe	8 $\uparrow\downarrow$	8 $\uparrow\downarrow$	17 $\uparrow\downarrow$	9.6 $\uparrow\downarrow$

^aMC simulation based on J_s from Ref. 29.^bReference 56.^cGround state depends on initialization of MC simulation.

hybrid functionals capture the correct magnetic ground state: EuO and EuS are ferromagnetic, and EuTe is antiferromagnetic. For EuSe, the ordering temperature is very small due to the competition of the nn and the nnn interaction. In the HSE functional, this gives rise to different magnetic ground states, depending on the starting point of the MC simulation. Within the hybrid-functional calculations, we predict the magnetic ground state correctly for the whole series. We observe a tendency towards too large values for the ordering temperatures as compared with the experimental ones, caused by the overestimation of most of the magnetic interaction strengths (Table V).

Conducting MC simulations with the coupling constants from a LDA + U approach,²⁹ on the other hand, we find that the tendency towards antiferromagnetic alignment is strongly overestimated. In contrast to experiment and our calculations, EuS aligns antiferromagnetically and the ordering temperatures for EuSe and EuTe are too large.

When expressed on an energy scale, the critical temperatures of these systems range from 1 to 5 meV. Considering these small values, we find a rather reasonable agreement between the experimental observations and our parameter-free theoretical predictions, because the calculations are subject to the following uncertainties: (i) We converged the total energy differences in Eqs. (2) and (3) up to 1 meV, which corresponds to a possible error in the critical temperatures of 3 K. (ii) The critical temperature determined from the Monte Carlo simulation differs slightly from other theoretical approaches, e.g., the random-phase approximation, which may be associated to an error of roughly 10%.⁴¹ (iii) The thermal expansion of the compounds between 0 K and the magnetic ordering temperature may account for an additional change in the coupling strength. Evaluating the coupling strengths once at the liquid-helium and once at the room-temperature lattice constant, we find that this expansion of the lattice constant is associated to a decrease of the Curie temperature in EuO of roughly 10 K. (iv) For a better description of the strongly localized f electrons in Eu, a slightly larger fraction of Hartree-Fock could be more suitable, which would decrease the ordering temperature. (v) Furthermore, we neglected the interaction with the third-nearest and further neighbors, which may additionally change the ordering temperature. As the strength of the couplings oscillates in a RKKY-like pattern, it is hard to estimate the impact on the magnetic ordering temperatures.

IV. CONCLUSIONS

In this work we have demonstrated that the PBE0 and HSE hybrid functionals provide a parameter-free alternative to the DFT + U approach for the Eu chalcogenides. In detail, the theoretical lattice constants fit very well to those from experiment. The bulk moduli are at the lower end of the experimental values, but well within the experimental error bars. In the description of the electronic band structure, hybrid functionals overcome the ambiguity associated with the size of the Hubbard U parameter in the DFT + U approach and improve the qualitative and in most cases even the quantitative agreement with experiment. In PBE0 and HSE, the band transitions of the europium chalcogenides are in agreement to the experiment at several scientifically relevant points in the Brillouin zone: The lowest transition is of indirect nature (Γ -X) and the lowest direct band transition is situated at the X point. The PBE0 and the HSE functional, respectively, over- and underestimate the size of the band gaps in comparison to the experiment. This is associated to the almost dispersionless shift of the conduction band states by 0.7 eV between the two hybrid functionals. The bandwidth of the p states and the transition from these states to the conduction band is described qualitatively correctly, although the trend towards delocalization of the p wave function is underestimated in size.

In great difference to the local functionals, the hybrid functionals describe the magnetic phases as well as the trend

of the critical temperatures and of the magnetic interactions between neighboring europium sites correctly across the Eu chalcogenide series. Even the complexity of the magnetic ground state in EuSe is captured correctly. With our simple model including only the exchange coupling between nearest and next-nearest Eu neighbors and ignoring the temperature expansion of the lattice, we obtain ordering temperatures whose errors are equivalent to less than 2 meV. In general, the magnetic interactions between neighboring europium atoms are overestimated by hybrid functionals resulting in too large values of the ordering temperatures. Compared with the LDA + U approach, we find an improved description of the magnetic ground state particularly for the heavier chalcogenides.

The success of the hybrid functionals are in line with our previous investigation on GdN,⁴¹ and we speculate that this is a general feature of the hybrid functionals that can be transferred to a wide class of ordered and disordered rare-earth compounds, multilayers, heterostructures, and surfaces.

ACKNOWLEDGMENTS

We would like to thank Phivos Mavropoulos for his assistance in performing the Monte Carlo simulations and gratefully acknowledge the funding by the Young Investigators Group Programme of the Helmholtz Association (“Computational Nanoferronics Laboratory,” Contract VH-NG-409).

*martin.schlipf@gmail.com

¹B. T. Matthias, R. M. Bozorth, and J. H. Van Vleck, *Phys. Rev. Lett.* **7**, 160 (1961).

²T. R. McGuire, B. E. Argyle, M. W. Shafer, and J. S. Smart, *Appl. Phys. Lett.* **1**, 17 (1962).

³P. Wachter, *Crit. Rev. Solid State Sci.* **3**, 189 (1972).

⁴B. Díaz, E. Granado, E. Abramof, L. Torres, R. T. Lechner, G. Springholz, and G. Bauer, *Phys. Rev. B* **81**, 184428 (2010).

⁵X. Hao, J. S. Moodera, and R. Meservey, *Phys. Rev. B* **42**, 8235 (1990).

⁶T. S. Santos and J. S. Moodera, *Phys. Rev. B* **69**, 241203 (2004).

⁷T. J. Konno, N. Ogawa, K. Wakoh, K. Sumiyama, and K. Suzuki, *Jpn. J. Appl. Phys.* **35**, 6052 (1996).

⁸A. Schmehl, V. Vaithyanathan, A. Herrnberger, S. Thiel, C. Richter, M. Liberati, T. Heeg, M. Ruckerath, L. F. Kourkoutis, S. Muhlbauer, P. Boni, D. A. Muller, Y. Barash, J. Schubert, Y. Idzerda, J. Mannhart, and D. G. Schlom, *Nat. Mater.* **6**, 882 (2007).

⁹C. Caspers, M. Müller, A. X. Gray, A. M. Kaiser, A. Gloskovskii, C. S. Fadley, W. Drube, and C. M. Schneider, *Phys. Status Solidi-R* **5**, 441 (2011).

¹⁰R. Sutarto, S. G. Altendorf, B. Coloru, M. Moretti Sala, T. Haupricht, C. F. Chang, Z. Hu, C. Schüßler-Langeheine, N. Hollmann, H. Kierspel, J. A. Mydosh, H. H. Hsieh, H.-J. Lin, C. T. Chen, and L. H. Tjeng, *Phys. Rev. B* **80**, 085308 (2009).

¹¹A. G. Swartz, J. Ciraldo, J. J. I. Wong, Y. Li, W. Han, T. Lin, S. Mack, J. Shi, D. D. Awschalom, and R. K. Kawakami, *Appl. Phys. Lett.* **97**, 112509 (2010).

¹²A. Mauger and C. Godart, *Phys. Rep.* **141**, 51 (1986).

¹³M. W. Shafer and T. R. McGuire, *J. Appl. Phys.* **39**, 588 (1968).

¹⁴K. Y. Ahn and T. R. McGuire, *J. Appl. Phys.* **39**, 5061 (1968).

¹⁵T. Matsumoto, K. Yamaguchi, M. Yuri, K. Kawaguchi, N. Koshizaki, and K. Yamada, *J. Phys.: Condens. Matter* **16**, 6017 (2004).

¹⁶H. Ott, S. J. Heise, R. Sutarto, Z. Hu, C. F. Chang, H. H. Hsieh, H.-J. Lin, C. T. Chen, and L. H. Tjeng, *Phys. Rev. B* **73**, 094407 (2006).

¹⁷H. Miyazaki, H. J. Im, K. Terashima, S. Yagi, M. Kato, K. Soda, T. Ito, and S. Kimura, *Appl. Phys. Lett.* **96**, 232503 (2010).

¹⁸P. Liu, J. Tang, J. A. C. Santana, K. D. Belashchenko, and P. A. Dowben, *J. Appl. Phys.* **109**, 07C311 (2011).

¹⁹O. Massenet, Y. Capiomont, and N. V. Dang, *J. Appl. Phys.* **45**, 3593 (1974).

²⁰D. E. Shai, A. J. Melville, J. W. Harter, E. J. Monkman, D. W. Shen, A. Schmehl, D. G. Schlom, and K. M. Shen, *Phys. Rev. Lett.* **108**, 267003 (2012).

²¹G. Busch and P. Wachter, *Phys. Condens. Matter* **5**, 232 (1966).

²²W. Nolting and A. Olés, *Z. Phys. B Condens. Matter* **43**, 37 (1981).

²³M. Arnold and J. Kroha, *Phys. Rev. Lett.* **100**, 046404 (2008).

²⁴P. Hohenberg and W. Kohn, *Phys. Rev.* **136**, B864 (1964).

²⁵W. Kohn and L. J. Sham, *Phys. Rev.* **140**, A1133 (1965).

²⁶E. Engel, in *A Primer in Density Functional Theory*, edited by C. Fiolhais, M. A. L. Marques, and F. Nogueira (Springer, Berlin, 2003), Chap. 2, pp. 56–143.

²⁷V. I. Anisimov, F. Aryasetiawan, and A. I. Lichtenstein, *J. Phys.: Condens. Matter* **9**, 767 (1997).

- ²⁸J. Kunes, W. Ku, and W. E. Pickett, *J. Phys. Soc. Jpn.* **74**, 1408 (2005).
- ²⁹P. Larson and W. R. L. Lambrecht, *J. Phys.: Condens. Matter* **18**, 11333 (2006).
- ³⁰N. J. C. Ingle and I. S. Elfimov, *Phys. Rev. B* **77**, 121202 (2008).
- ³¹J. M. An, S. V. Barabash, V. Ozolins, M. van Schilfgaarde, and K. D. Belashchenko, *Phys. Rev. B* **83**, 064105 (2011).
- ³²M. Cococcioni and S. de Gironcoli, *Phys. Rev. B* **71**, 035105 (2005).
- ³³E. Şaşıoğlu, C. Friedrich, and S. Blügel, *Phys. Rev. B* **83**, 121101(R) (2011).
- ³⁴J. P. Perdew, M. Ernzerhof, and K. Burke, *J. Chem. Phys.* **105**, 9982 (1996).
- ³⁵J. Heyd, G. E. Scuseria, and M. Ernzerhof, *J. Chem. Phys.* **118**, 8207 (2003).
- ³⁶A. D. Becke, *J. Chem. Phys.* **98**, 1372 (1993).
- ³⁷A. D. Becke, *J. Chem. Phys.* **98**, 5648 (1993).
- ³⁸C. Friedrich, A. Schindlmayr, and S. Blügel, *Comput. Phys. Commun.* **180**, 347 (2009).
- ³⁹<http://www.flapw.de>
- ⁴⁰M. Betzinger, C. Friedrich, and S. Blügel, *Phys. Rev. B* **81**, 195117 (2010).
- ⁴¹M. Schlipf, M. Betzinger, C. Friedrich, M. Ležaić, and S. Blügel, *Phys. Rev. B* **84**, 125142 (2011).
- ⁴²M. Betzinger, C. Friedrich, S. Blügel, and A. Görling, *Phys. Rev. B* **83**, 045105 (2011).
- ⁴³F. Murnaghan, *Proc. Natl. Acad. Sci. USA* **30**, 244 (1944).
- ⁴⁴P. Larson, W. R. L. Lambrecht, A. Chantis, and M. van Schilfgaarde, *Phys. Rev. B* **75**, 045114 (2007).
- ⁴⁵K. Binder and D. W. Heermann, *Monte Carlo Simulation in Statistical Physics An Introduction* (Springer, Berlin, 2010).
- ⁴⁶F. Lévy, *Phys. Condens. Matter* **10**, 71 (1969).
- ⁴⁷Collaboration: Authors and editors of the volumes III/17G-41D, in *Non-Tetrahedrally Bonded Binary Compounds II*, Vol. 41D of *Landolt-Börnstein - Group III Condensed Matter*, edited by O. Madelung, U. Rössler, and M. Schulz (Springer, Berlin, 2000).
- ⁴⁸N. Marzari and D. Vanderbilt, *Phys. Rev. B* **56**, 12847 (1997).
- ⁴⁹J. R. Yates, X. Wang, D. Vanderbilt, and I. Souza, *Phys. Rev. B* **75**, 195121 (2007).
- ⁵⁰F. Freimuth, Y. Mokrousov, D. Wortmann, S. Heinze, and S. Blügel, *Phys. Rev. B* **78**, 035120 (2008).
- ⁵¹J. K. Lang, Y. Baer, and P. A. Cox, *J. Phys. F: Met. Phys.* **11**, 121 (1981).
- ⁵²H. Yamada, T. Fukawa, T. Muro, Y. Tanaka, S. Imada, S. Suga, D.-X. Li, and T. Suzuki, *J. Phys. Soc. Jpn.* **65**, 1000 (1996).
- ⁵³P. G. Steeneken, L. H. Tjeng, I. Elfimov, G. A. Sawatzky, G. Ghiringhelli, N. B. Brookes, and D.-J. Huang, *Phys. Rev. Lett.* **88**, 047201 (2002).
- ⁵⁴J. P. Perdew, K. Burke, and M. Ernzerhof, *Phys. Rev. Lett.* **77**, 3865 (1996).
- ⁵⁵C. Friedrich, M. Betzinger, M. Schlipf, S. Blügel, and A. Schindlmayr, *J. Phys.: Condens. Matter* **24**, 293201 (2012).
- ⁵⁶U. Köbler and C. Sauer, *Magnetic and Other Properties of Oxides and Related Compounds - Part C*, Vol. 12 of *Landolt-Börnstein - Group III Condensed Matter* (Springer, Berlin, 1982).